In-cylinder Flow Evolution using Tomographic PIV in an Internal Combustion Engine

Article *in* Journal of Energy Resources Technology, Transactions of the ASME · August 2017

DOI: 10.1115/1.4037686

3 authors:

Avinash Kumar Agarwal
Indian Institute of Technology Kanpur
581 PUBLICATIONS **23,176** CITATIONS

SEE PROFILE

Suresh Gadekar
Indian Institute of Technology Kanpur
4 PUBLICATIONS **67** CITATIONS

SEE PROFILE

Akhilendra Pratap Singh
Indian Institute of Technology Kanpur
102 PUBLICATIONS **3,600** CITATIONS

SEE PROFILE

In-Cylinder Flow Evolution Using Tomographic Particle Imaging Velocimetry in an Internal Combustion Engine

Avinash Kumar Agarwal[1]
Engine Research Laboratory,
Department of Mechanical Engineering,
Indian Institute of Technology Kanpur,
Kanpur 208016, India
e-mail: akag@iitk.ac.in

Suresh Gadekar
Engine Research Laboratory,
Department of Mechanical Engineering,
Indian Institute of Technology Kanpur,
Kanpur 208016, India
e-mail: srshgdkr@gmail.com

Akhilendra Pratap Singh
Engine Research Laboratory,
Department of Mechanical Engineering,
Indian Institute of Technology Kanpur,
Kanpur 208016, India
e-mail: akhips@iitk.ac.in

In-cylinder flows in internal combustion (IC) engines have always been a focus of study in order to gain better understanding of fuel–air mixing process and combustion optimization. Different conventional experimental techniques such as hot wire anemometry (HWA), laser Doppler anemometry (LDA), and numerical simulations have been grossly inadequate for complete understanding of the complex 3D flows inside the engine cylinder. In this experimental study, tomographic particle imaging velocimetry (PIV) was applied in a four-valve, single-cylinder optical research engine, with an objective of investigating the in-cylinder flow evolution during intake and compression strokes in an engine cycle. In-cylinder flow seeded with ultra-fine graphite particles was illuminated by a high energy, high frequency Nd:YLF laser. The motion of these tracer particles was captured using two cameras from different viewing angles. These two-directional projections of flowfield were used to reconstruct the 3D flowfield of the measurement volume ($36 \times 25 \times 8$ mm^3), using multiplicative algebraic reconstruction technique (MART) algorithm. Captured images of 50 consecutive engine cycles were ensemble averaged to analyze the in-cylinder flow evolution. Results indicated that the in-cylinder flows are dependent on the piston position and spatial location inside the engine cylinder. The randomness of air-flow fields during the intake stroke was very high, which became more homogeneous during the compression stroke. The flows were found to be highly dependent on Z plane location inside the engine. During the intake stroke, flows were highly turbulent throughout the engine cylinder, and velocities vectors were observed in all directions. However, during the compression stroke, flow velocities were higher near the injector, and they reduced closer to the valves. Absolute velocity during compression stroke was mainly contributed by the out of plane velocity (V_z) component.
[DOI: 10.1115/1.4037686]

Keywords: flow visualization, turbulent kinetic energy, velocity component analysis, vorticity analysis

Introduction

In the last few decades, automotive researchers have adopted methodologies such as turbocharging, exhaust gas recirculation, electronically controlled high-pressure fuel injection, multiple injections, etc., to avoid conditions favorable for formation of harmful emissions in the engine combustion chamber [1]. However, formation of harmful pollutants in diesel engines is significantly affected by fuel's spray characteristics, fuel–air mixing processes, and consequently the combustion [2,3]. Researchers are continuously improving their understanding of in-cylinder processes and reported that homogeneous fuel–air mixing improved engine emission characteristics [4]. In-cylinder air-flow mainly influences fuel–air mixing that subsequently affects the combustion. Several studies report the existence of specific flow conditions which result in optimal engine operation [5,6]. Therefore, in order to understand fuel–air mixing processes, it is essential to analyze in-cylinder flow evolution and spatial flow structures in order to obtain optimal engine performance. With limited applicability of numerical simulations, flow analysis techniques such as hot wire anemometry (HWA) and laser Doppler anemometry (LDA) have been employed for understanding in-cylinder engine flows. Semenov performed one of the first studies for in-cylinder flows, where HWA was used to analyze flow pattern at different crank angle positions [7]. Tutak and Jamrozik [8] and Catania et al. [9] also used HWA to analyze the turbulent field around the cylinder axis and near the cylinder surface. However, intrusive nature of HWA and its inability to visualize three-dimensional air-flow structures limited its application for complex flow evolutions such as inside internal combustion (IC) engines. LDA is another non-intrusive flow measurement technique, which was used for in-cylinder flow analysis in IC engines. Kang and Back [10] studied tumble formation and decay of flow energy using LDA, whereas Driver et al. [11] used LDA for unsteady flow measurements inside the engine cylinder. These techniques measured the in-cylinder fluid flows, only at few locations and were capable of evaluating the volumetric flow structures instantaneously. Therefore, researchers were attracted to use particle imaging velocimetry (PIV) for understanding complex in-cylinder flow evolution in IC engines. PIV is a non-intrusive, multi-point flow measurement technique, which is capable of resolving issues faced by other techniques. In this optical flow visualization and measurement technique, in-cylinder flow field is illuminated at

[1]Corresponding author.

Contributed by the Internal Combustion Engine Division of ASME for publication in the JOURNAL OF ENERGY RESOURCES TECHNOLOGY. Manuscript received April 28, 2017; final manuscript received August 7, 2017; published online September 12, 2017. Editor: Hameed Metghalchi.

two instances with a short time lag between them. The illuminated flow field is captured using high-speed camera to obtain the flow information, after processing the acquired images. Application of PIV in IC engines is also associated with several practical experimental difficulties such as gaining optical access into the engine cylinder, providing a guiding path for the illuminating light sheet, choice of seeder particles, and directional ambiguity. Some of these issues have been already resolved. Various researchers discussed the methods for making proper choice of seeder particles for specific experimental conditions and effectiveness of a particular image evaluation method [12,13]. Disch et al. [14] carried out endoscopic measurements of air-flow behavior through an optical access in an IC engine. Limitations related to optical access, physical space surrounding the engine, thick curved glass cylinder, and engine vibrations caused major issues in PIV measurements and affected the accuracy of experimental results.

Despite numerous challenges with the optical access, uniform seeding of intake air and guiding the illuminating light, several researchers have successfully implemented PIV to study the IC engine flows. Nishiyama et al. [15] applied endoscopic PIV measurement to study the exhaust manifold flows. In another study for gas velocity measurement, in-cylinder access was gained through the fuel injector port and exhaust valves [16]. Reeves et al. [17] used 2D digital PIV for quantification of major air-flow structures at different crank angle positions. To gain understanding of evolution of 3D flowfield, planar PIV has been applied in different planes inside the engine cylinder. Dannemann et al. [18] applied planar PIV in eight different vertical planes and reported a reduction in spatial variation of flowfield with the crank angle position. The experimental results obtained from planer PIV measurements were used for validation of simulations and modeling results. Das [19] also used vertical plane PIV data for KIVA model validation. However, existence of strong out of plane velocity components and complex 3D flow structures makes it very challenging to understand the in-cylinder flow evolution and its spatial variations. Such volumetric flowfields can be studied by holographic PIV (TPIV), which was developed by Elsinga et al. [20]. Tomographic PIV is another type of three-dimensional three component (3D-3C) velocity measurement technique. Basic principle used for velocity measurement is the same as 2D PIV, except that the flow field projections are captured by several cameras. This technique uses a tomographic reconstruction, which consists of reconstruction of 3D objects from a set of its 2D projections. TPIV uses multiplicative algebraic reconstruction technique (MART) to construct the 3D flowfield [21]. Baum et al. [22] calculated uncertainty in TPIV measurements in IC engines using the principle of mass conservation and found a precision of ~9%, which is same as generic TPIV configurations. Overbrueggen et al. [23,24] performed in-cylinder measurement of whole volume of the intake flow of a four valve engine at 160-deg crank angle. They used 2C PIV measurement in several planes, 3C PIV measurement in a set of planes in addition to holographic PIV measurements. They analyzed the flowfields by distribution of velocity field, turbulent kinetic energy (TKE), and vortex identification functions. Singh et al. [25] performed TPIV experiments in an IC engine at different engine speeds and different in-cylinder locations. They reported that different velocity components affect flow characteristics in a specific manner and each component dominate other components, depending on the piston position and in-cylinder location. Singh et al. [26] further extended the experiments to examine the effect of different engine operating parameters such as engine speed, intake air temperature, and intake port deactivation on the in-cylinder flow evolution. They detected great dependence of these parameters on different flow characteristics such as absolute velocity, vorticity, TKE, etc.

This study is a further extension of these two studies and presents 3D, in-cylinder flow evolution in a single cylinder, four-valve, optical diesel engine at 1200 rpm. Three-dimensional and 2D flowfields are presented at different crank angle positions during the intake and compression stokes, and an average of 50 consecutive engine cycles is used to eliminate the effect of cyclic variations. Variations in *Z*-direction component of absolute velocity and its variations in different vertical locations on the *Z*-axis have also been presented, especially at mid-intake and mid-compression stroke locations.

Table 1 Technical specifications of the single cylinder optical research engine

Engine characteristics	Specifications
Model	AVL 5402.070
Bore/stroke	85 mm/90 mm
Swept volume	510.7 cm^3
Inlet port geometry	Tangential and swirl inlet ports
Engine management system	AVL-RPEMS + ETK-7
Fuel injection pressure	Up to 1400 bar
Injector nozzle	DSLA142P
Maximum engine speed	3000 rpm
Maximum in-cylinder pressure	60 bar
Valves per cylinder	4 (2 inlet, 2 exhaust)
Liner type (base)	Wet
Liner type (optical)	Dry
Engine rotation	Clockwise
Nominal swirl ratio	1.78

Experimental Setup

For studying the flow evolution in the engine cylinder, TPIV was implemented in a four-valve, single cylinder optical research engine. This test engine has two intake ports, namely a swirl port and a tangential port. The swirl port, more commonly known as helical port, provides helical pattern to the intake air-flow around the valve axis before the air enters the cylinder and generates swirling flow pattern upstream of the intake valve. The tangential port is a flow directing port, which generates swirl by forcing the flow around the circumference of the intake valve with angular momentum about the cylinder axis. The optical access inside the engine cylinder was obtained through a 30 mm high, 19 mm thick transparent quartz liner, which could sustain a peak firing pressure upto 90 bar. The illuminating light was guided into the engine cylinder using a 45-deg inclined mirror, which was placed inside the extended piston. A flat sapphire window was fixed in the piston bowl (diametrical dimension of 40 mm), which allowed the illuminating light into the combustion chamber. Details of test engine are given in Table 1, and the schematic of the experimental setup is given in Fig. 1.

Important specifications of PIV and visualization systems are given in Table 2.

In this study, engine was operated in the motoring mode using a transient dynamometer (Wittur Electric Drives; 2SB 3) at 1200 rpm. The intake air was normally aspirated at room temperature (35 °C). Graphite seeder particles (particle diameter of ~1 μm) were put into the intake air stream using a seed particle dispenser. Size of graphite particles was selected in such a way that they followed the air flow faithfully and scattered enough light for capturing by the camera. For illumination of graphite particles, a high-energy, diode-pumped, dual-cavity Nd:YLF laser was used. The laser beam was redirected by mirrors and transformed into a laser sheet using a collimator, which was further guided into the engine cylinder using reflecting mirrors placed appropriately. The illuminated flow field was captured by the two high-speed cameras (charge-coupled device 12 bit camera), which were operated in double frame mode at 4000 fps. Cameras were placed to view the measurement volume from different directions (Fig. 2).

To get proper focus on the flow field volume, cameras were equipped with Scheimpflugs. The interframe time separation was fixed at 10 μs so that none of high-velocity particles crossed critical distance (1/4th of the interrogation window) and goes out of visualization zone. A high-speed controller was used to synchronize the camera with double-pulsed laser so that the images were

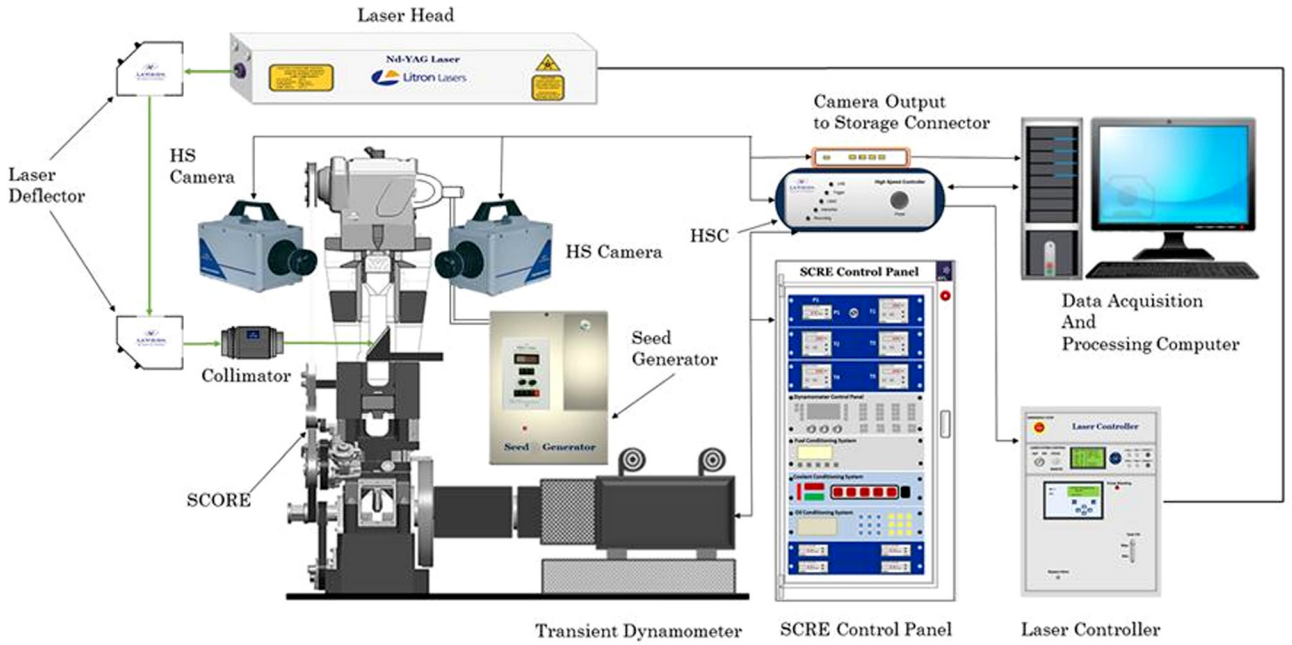

Fig. 1 Experimental setup for TPIV investigations in a single cylinder optical research engine

Table 2 Technical specifications of the PIV and visualization systems

Specifications of seed dispenser	
Make/model	Palas/RBG 1000
Particle dispenser	Solid particle dispenser
Seeding material	Graphite Particles
Average seed size	~5 μm
Dispersion gas	Dry compressed air
Specifications of camera	
Make/model	La-Vision; high-speed star 6.0
Imaging sensor	CMOS
Sensor resolution	1024 × 1024 pixels
Pixel size	20 μm
Frame rate	4000 Hz
Lens mount	F mount (Nikon)
Recording gray scale	Monochrome 12 bits, Color: 12 bits each on RGB
Trigger signal input	TTL
Specifications of high-speed controller	
Make/model	La-Vision/high-speed controller
Time resolution	10 ns
Typical jitter between all outputs	<1 ns
Trigger source	Internal generator, external TTL input or rotary encoder signals
Image trigger	Internal/asynchronous, external/hyper-sampling
Device	Multiple HS cameras, A/D-convertor, IRO, E-monitor, laser
Version	USB
Digital output	Opto coupled TLL
Specifications of high-speed laser	
Make/model	Litron/LDY series
Maximum energy	150 W
Maximum frequency	10 kHz
Trigger source	Internal generator, external TTL input
Class	Diode pumped, dual cavity class 4 laser

recorded at the instant of flow illumination. For timely acquisition of images, piston or crank angle position (resolution = 0.5 crank angle degree (CAD)) and cycle trigger signals were obtained using precision optical shaft encoder. Acquisition cycle trigger and image triggers were generated by high-speed controller according to the acquisition inputs. DAVIS software was used for providing these inputs. Photographic displacements of the acquired images were transferred to the global coordinates and physical displacements using calibration. Calibration was performed by placing a double layer calibration plate at the center of the measurement volume and by using a third-order polynomial calibration model.

Image Processing

Acquired flowfield images were pre-processed and post-processed to obtain final velocity profiles in the measurement

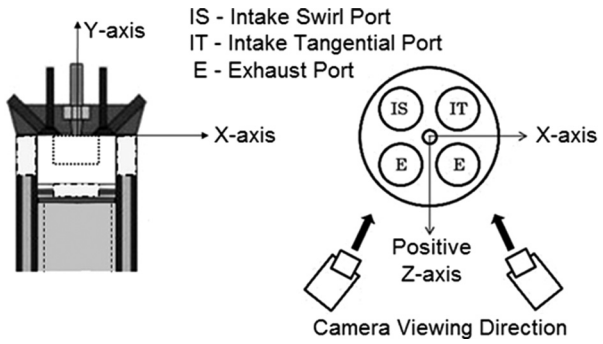

Fig. 2 Coordinate system, camera viewing directions, and port locations

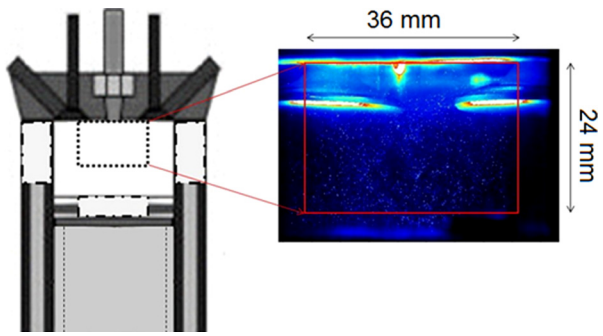

Fig. 3 Area of interest for in-cylinder flow characterization

volume. Pre-processing steps involved subtraction of sliding minimum intensity, Gaussian smoothening, sharpening, and application of masks to extract exact area of interest (AoI). In post-processing, these pre-processed images or 2D projections of the flowfield were used to reconstruct the 3D volume using multiplicative algebraic reconstruction technique (MART). Further the reconstructed 3D volume was cross-correlated with decreasing interrogation volume from 128×128 pixels to 32×32 pixels with 75% overlap between the interrogation windows. In case of any data loss in small volumes, an average data of neighboring volume of $5 \times 5 \times 5$ voxel was inserted. Any absurd vectors in comparison to their neighboring vectors were removed. Finally, the velocity vectors were smoothened using Gaussian smoothening.

In this study, flowfield images were acquired in the intake and compression stroke for 50 consecutive thermodynamic engine cycles in a crank angle range of 320-deg CA bTDC to 40-deg CA bTDC and a resolution of 2 CAD. All crank angle positions were referenced with respect to firing top dead center (TDC) position. A suitable AoI of $38 \times 25 \times 8$ mm^3 at the center of engine cylinder was chosen from the area of overlap between the two cameras (Fig. 3). The coordinate system (origin at the injector tip) and AoI used in this study is shown in Figs. 2 and 3, respectively.

Results and Discussion

Air-flow characteristics of an IC engine depends on several factors such as engine speed, valve lift, and piston position. During the intake stroke, air-flow is known to be turbulent and heterogeneous compared to the compression stroke. High-velocity zones are normally observed close to the intake valves. As the cycle progresses, air-flow structures of the intake stroke interact with piston top as well as the cylinder walls, dissipating the turbulent flow energy and breaking down the larger structures into smaller structures. This leads to uniform flow during the compression stroke.

Flow Evolution During the Intake Stroke. Figure 4 shows the in-cylinder flow structures developed during the intake stroke at different crank angle positions (320-deg, 290-deg, 270-deg, and 190-deg CA). Here, left side Fig. 4 shows absolute air velocity iso-surfaces formed inside the measurement volume, whereas the right-side images show the air velocity field in the central vertical plane, below the injector tip (at $z = 0$ mm). Lower right corner represents relative piston position and direction of its motion for the corresponding CA position. For 320-deg CA, piston occupies a certain area within the AoI thus flowfield is present in the remaining area (Figs. 4(*a*-i) and 4(*a*-ii)). For this crank angle position, valves are yet to fully open, leading to higher air velocities due to small annular gap between the valve and the valve seat. This high velocity air gets reflected after colliding with the cylinder walls. Reflected air field can be seen in the upper left corner of 3D flowfield (Fig. 4(*a*-i), flow enclosed in the light blue rectangle). Further, this reflected air collides with the incoming air, thus forming stagnation zone, which can also be observed at the top of 3D flowfield (Fig. 4(*a*-i)). At the center of the 2D flowfield, strong downward flow zone can be noticed, which is formed due to combined effect of both intake valves (Fig. 4(*a*-ii), black boundary region). This downward air jet strikes the piston top, and results in recirculation patterns on both sides of the incoming jet. As the cycle progresses, valve opening widens and piston further moves downward, pulling the high velocity incoming air into the middle of the cylinder volume. At 290-deg CA, complete AoI is occupied by the air and high velocity region can be located at the center of the cylinder (Fig. 4(*b*-i)). This high-velocity region between the intake valves was also reported by Foucher et al. [27]. The high-speed air travelling along the cylinder axis hits the piston and forms vertical tumble like structures. Generation of counter rotating vortices on both sides of cylinder axis can be seen in 2D flowfield in the center plane at 290-deg CA (Fig. 4(*b*-ii), at $x = -2$ mm, $y = -18$ mm, and $x = 8$ mm, $y = -14$ mm). The formation of such cyclic structures after the flow reversal from the piston was also reported by Deslandes et al. [28] and Lumley [29]. Further with valves properly lifted, piston speed plays an important role in flow evolution. At 240-deg CA, piston speed decreases, thus reducing the peak absolute velocity inside the engine cylinder (Fig. 4(*c*-i)). Leveling the center of vortices, these counter-rotating vortices become more symmetric about the cylinder axis (Fig. 4(*c*-ii)). With piston approaching bottom dead center, the flow reverses from the cylinder wall and piston becomes more dominant and most of intake generated large-scale flow structures disappear (190-deg CA, Figs. 4(*d*-i) and 4(*d*-ii)). This indicates dissipation of flow energy in the later part of the intake stroke.

Flow Evolution During the Compression Stroke. Figure 5 shows the flow evolution during the compression stroke. Comparison of the flowfields in the compression stroke with the intake stroke shows a significant reduction in absolute velocity. Thus for better visualization of small-scale flow structures, compression stroke velocity vector lengths were enlarged three-times compared to the intake stroke velocity vectors. Interactions between large-scale flows, piston top, and cylinder walls lead to viscous dissipation of TKE and breaking of these flow structures into smaller structures. During the compression stroke, vertical piston motion imparts additional momentum to the air thus pushing the air upward. At 140-deg CA, except near intake valves, almost uniform vertical air-flow can be seen in the entire measurement volume (Figs. 5(*a*-i) and 5(*a*-ii)).

At 90-degCA, absolute air velocity decreases and formation of several small vortical structures could be seen (Figs. 5(*b*-i) and 5(*b*-ii)). At this piston position, the velocity field is more homogeneous compared to any other piston position. Compressing flow near the cylinder head gets redirected toward the cylinder walls. Upward moving piston again covered certain areas of the AoI. At 40-deg CA, the velocity near the piston top became the maximum, making piston more important in the flow evolution during compression (Figs. 5(*c*-i) and 5(*c*-ii)). Here, flow near the cylinder

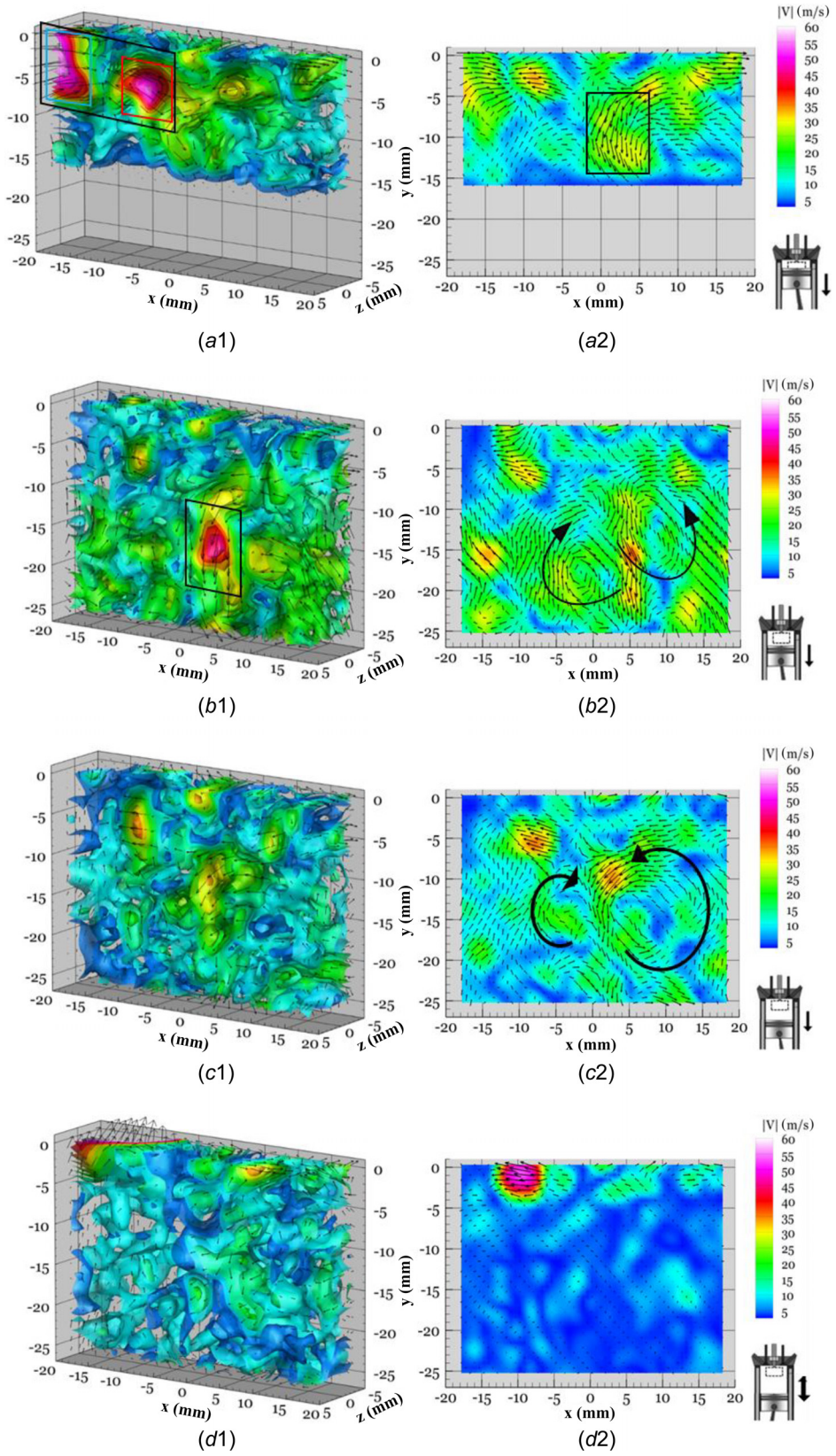

Fig. 4 Flow evolution during the intake stroke at 1200 rpm, obtained using TPIV at (*a*-i, *a*-ii) 320-deg CA, (*b*-i, *b*-ii) 290-deg CA, (*c*-i, *c*-ii) 240-deg CA, and (*d*-i, *d*-ii) 190-deg CA: (*a*-i) 3D view of flowfield at 320-deg CA, (*a*-ii) 2D plane at z = 0 at 320-deg CA, (*b*-i) 3D view of the flowfield at 290-deg CA, (*b*-ii) 2D plane at *z* = 0 at 290-deg CA, (*c*-i) 3D view of the flowfield at 240-deg CA, (*c*-ii) 2D plane at *z* = 0 at 240-deg CA, (*d*-i) 3-D view of the flowfield at 190-deg CA, and (*d*-ii) 2D plane at *z* = 0 at 190-deg CA

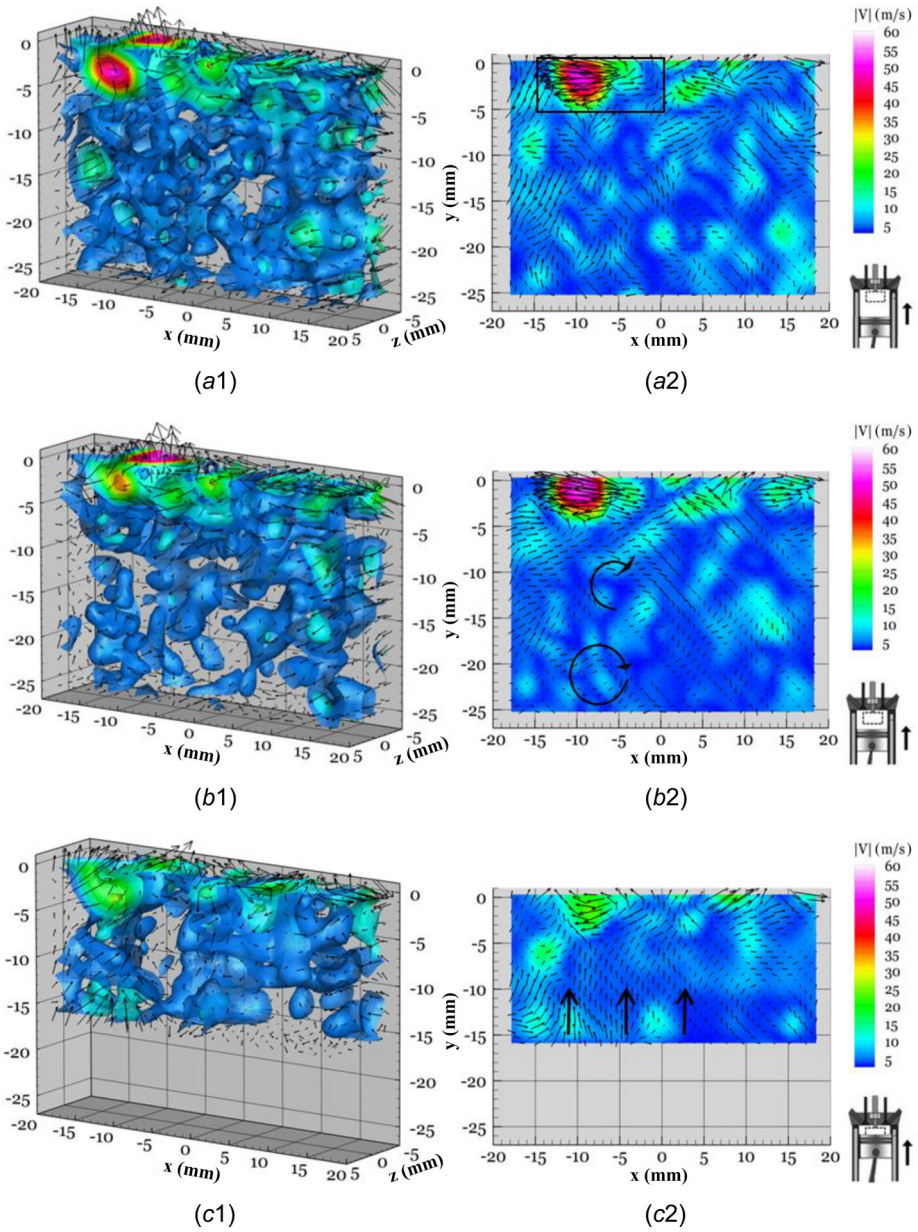

Fig. 5 Flow evolution during compression stroke at 1200 rpm, obtained using TPIV at (*a*-i, *a*-ii) 140-deg CA, (*b*-i, *b*-ii) 90-deg CA, and (*c*-i, *c*-ii) 40-deg CA: (*a*-i) 3D view of flowfield at 140-deg CA, (*a*-ii) 2D plane at $z = 0$ at 140-deg CA, (*b*-i) 3D view of the flowfield at 90-deg CA, (*b*-ii) 2D plane at $z = 0$ at 90-deg CA, (*c*-i) 3D view of the flowfield at 40-deg CA, and (*c*-ii) 2D plane at $z = 0$ at 40-deg CA

head was directed toward the cylinder walls indicating no sign of squish motion at this position. Thus, squish might be generated near the TDC position. Comparison of compression flow field with an intake flowfield shows significantly lower spatial variation in the compression stroke than in the intake stroke. This is in good correlation with reduction in spatial variations with respect to crank angle, as reported by Dannemann et al. [18]. They also reported relatively smoother flow distribution in the compression stroke compared to the intake stroke. Researchers also suggested that in-cylinder flows have highly three-dimensional characteristics; however, their observations were based on different vertical planes. They did not report any volumetric flow pattern.

Z-Directional Variation of the Absolute Velocity. Besides the engine speed and crank angle position of the given engine, in-cylinder flows are dependent on their spatial position in the cylinder. Higher spatial variation in the velocity results in formation of cyclic flows that subtly affect the fuel–air mixing. Figure 6 shows the spatial velocity variation at 270-deg CA (mid-intake stroke) in *Z*-direction, i.e., from intake valve side to the exhaust valve side. Here, $z = -4$ mm position is the closest to the intake valves, while $z = 4$ mm position is closer to the exhaust valves.

From the flowfields, it can be seen that higher velocities that were present near the intake valves (in the top region of the flowfield) have decayed towards the exhaust valve side. However, the central jet that was created by the combined action of both inlet ports, penetrated towards the exhaust side more strongly and was clearly seen in the center of all four planes. This central jet hit the piston top and got reflected in a vertically upward direction, and thus, the vertical component of velocity increased in *Z*-direction. From the flowfield, it can be seen that the exhaust side is prone to

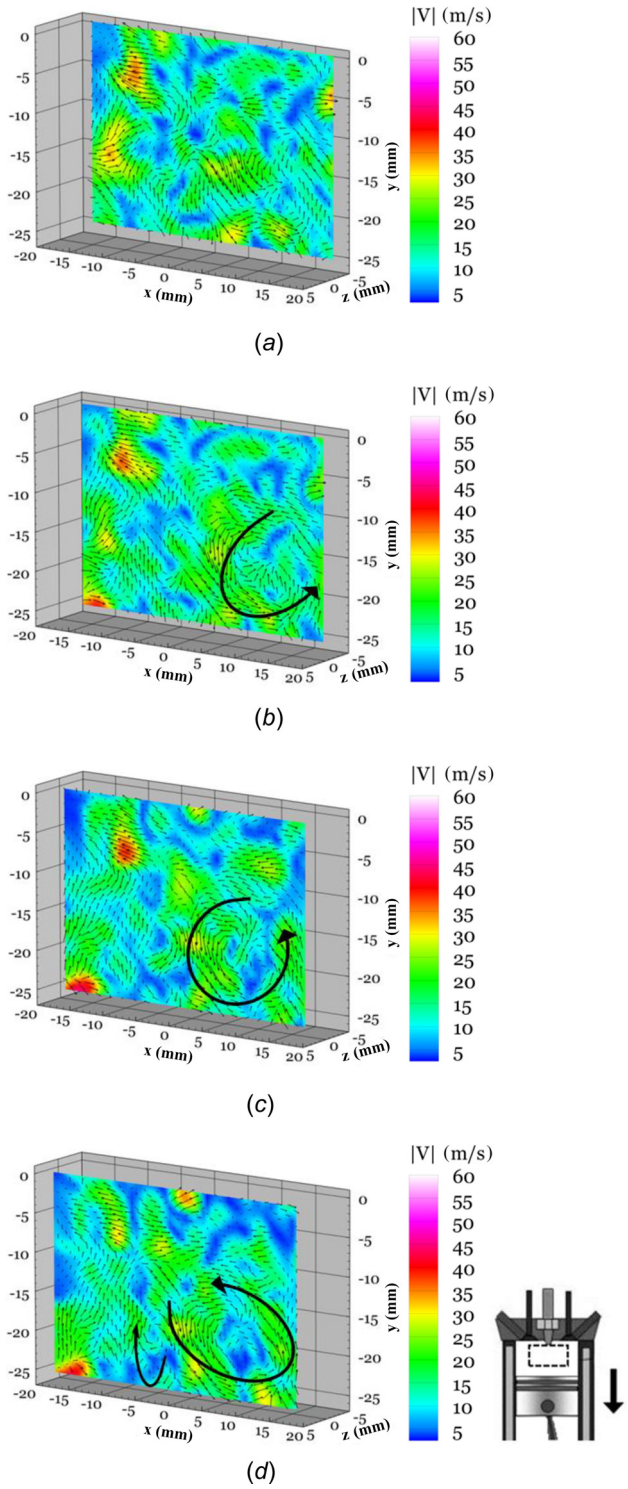

Fig. 6 ***Z*-directional variations in absolute velocity at 270-deg CA at 1200 rpm, obtained using TPIV at (*a*) $z = -4$ mm, (*b*) $z = -2$ mm, (*c*) $z = 2$ mm, and (*d*) $z = 4$ mm**

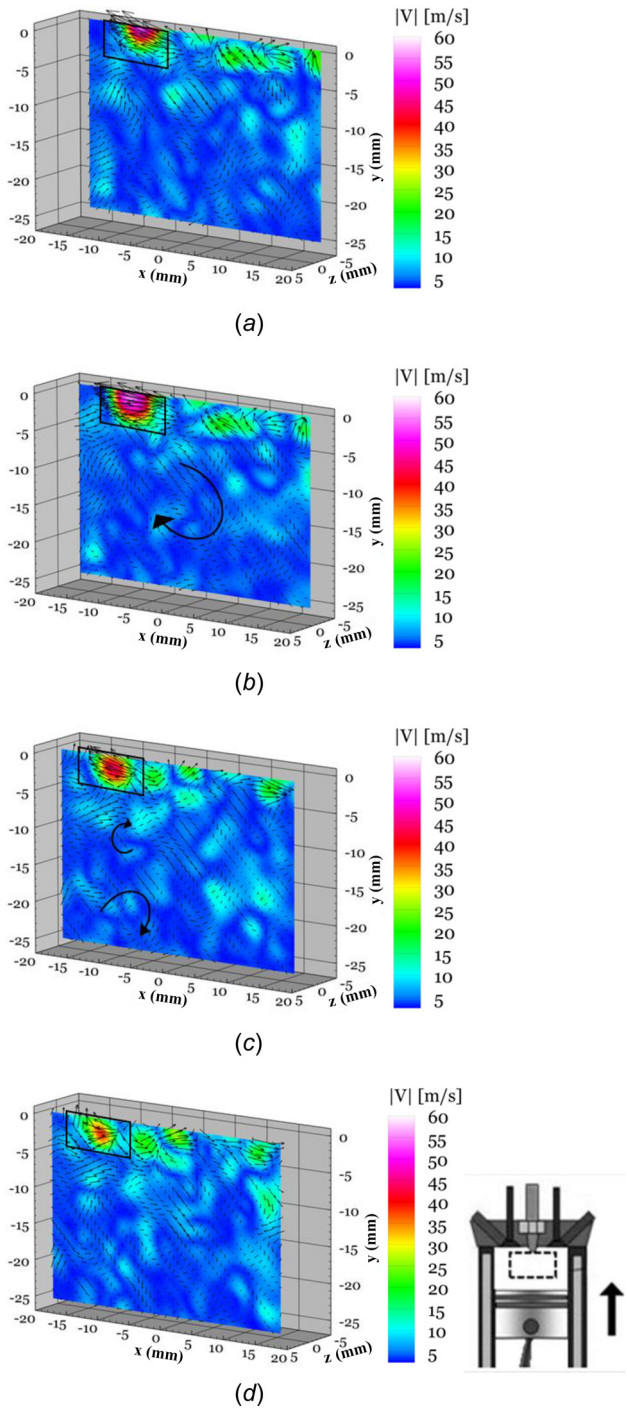

Fig. 7 ***Z*-directional variations in absolute velocity at 90-deg CA at 1200 rpm, obtained using TPIV at (*a*) $z = -4$ mm, (*b*) $z = -2$ mm, (*c*) $z = 2$ mm, and (*d*) $z = 4$ mm**

the formation of cyclical flow structures (Figs. 6(*c*) and 6(*d*)). This observation is a result of higher velocity gradient present in the exhaust, created by larger spatial variations.

Figure 7 shows similar spatial variations in mid-compression stroke (90-deg CA). Comparison of these results with earlier mid-intake stroke results showed that the velocities in compression stroke were significantly lower than the intake stroke velocities. Also flowfield is more homogeneous (except at locations near the cylinder head), and the cyclic structures of intake could not be located. Also from the velocity field of all planes, it could be observed that high velocities located around the cylinder head were stronger near the injector plane (vertical plane below injector, at $z = 0$ mm). The velocity magnitude decreased in positive and negative *Z*-direction, away from the injector plane. For the rest of the flowfield, velocity magnitude increased in the positive *Z*-direction, i.e., towards the exhaust valve. In addition, cyclic structures were noticed in the central zone, and the exhaust side was no longer prone to formation of cyclic structures.

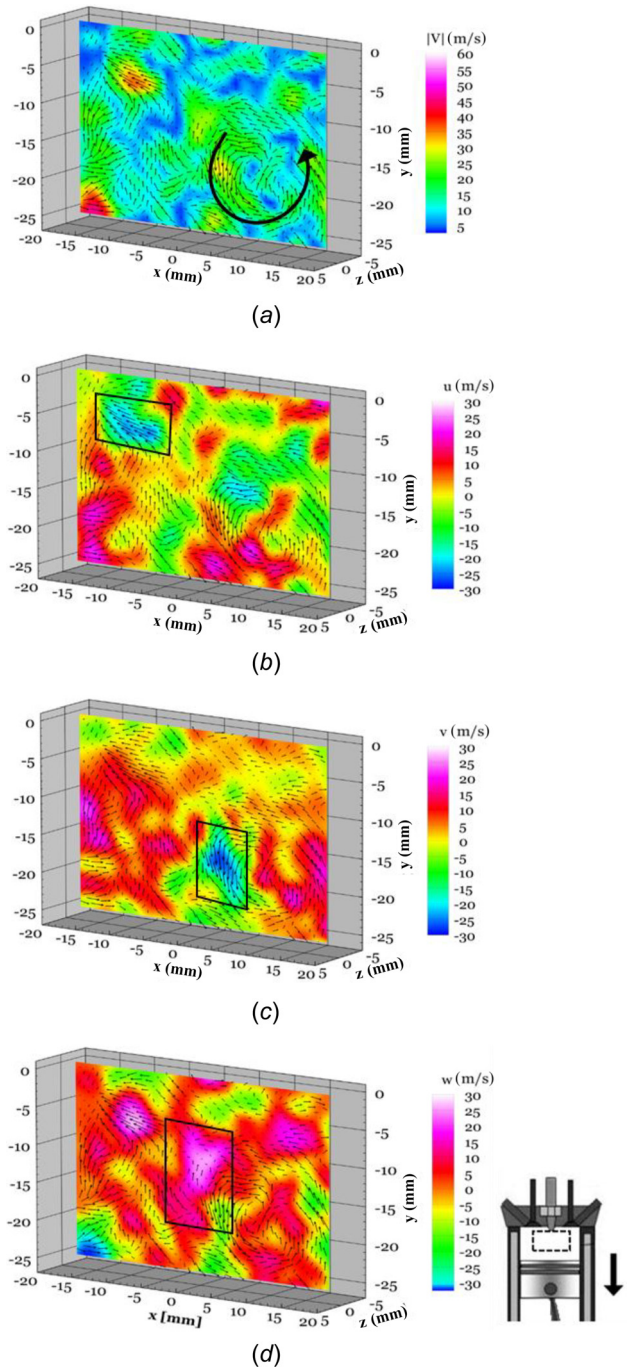

Fig. 8 Absolute velocity and its components at $z = 0$ mm 270-deg CA at 1200 rpm, for injector plane obtained using TPIV: (*a*) absolute velocity, (*b*) V_x component, (*c*) V_y component, and (*d*) V_z component

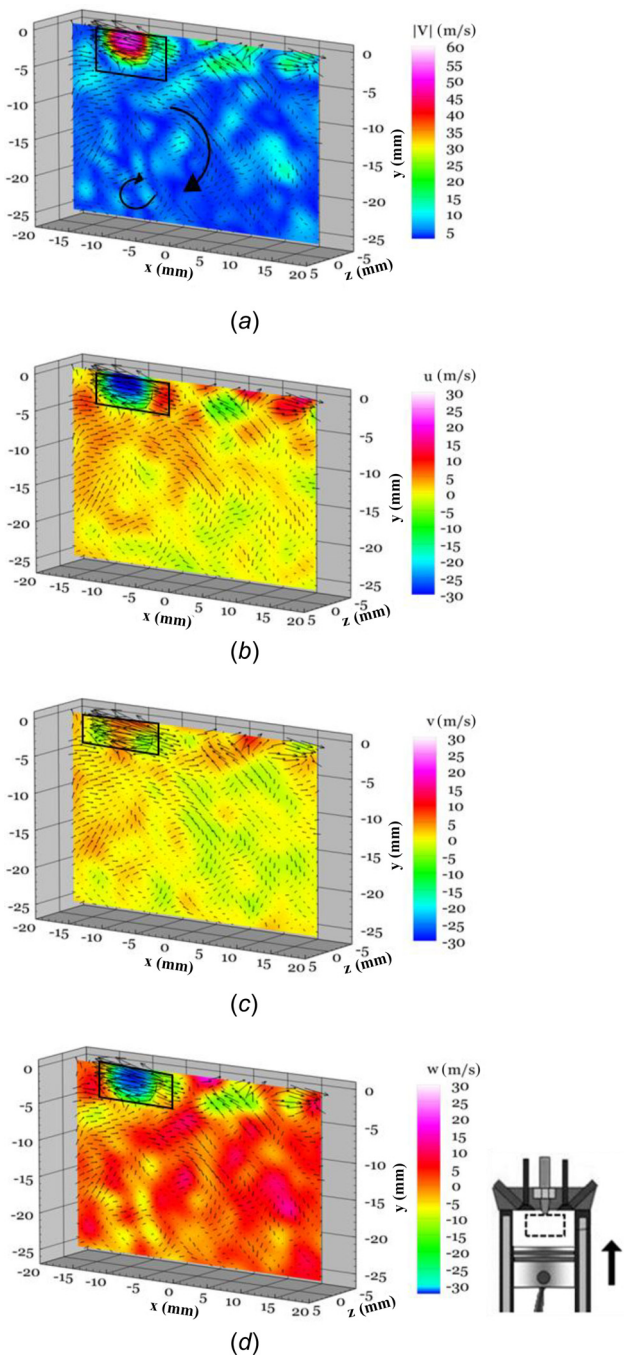

Fig. 9 Absolute velocity and its component at $z = 0$ mm, 90-deg CA at 1200 rpm, for injector plane obtained using TPIV: (*a*) absolute velocity, (*b*) V_x component, (*c*) V_y component, and (*d*) V_z component

Velocity Components. Ensemble average velocity and its components in the mid-intake and mid-compression positions in the injector plane are shown in Figs. 8 and 9, respectively. It can be noticed that at $z = 0$ mm, i.e., at the injector tip plane at 270-deg CA, the vortical structures are in continuity with $Z = 2$ mm and $Z = -2$ mm position (Figs. 6 and 8(*a*)). For V_x component, strong velocity field was present at the top and at the bottom regions of the measurement volume (Fig. 8(*b*)). High-velocity components in the top portion were a result of tangential velocity generated by the swirling port geometry and radial velocity of the valve surfaces, whereas in the bottom portion, high V_x was attributed to the reflections from the cylinder surfaces and the piston top. In case of V_y, high magnitude velocity components were present in the central region with vertical downward direction (Fig. 8(*c*)). These high downward velocity components were a result of intake jet, which penetrated the exhaust as seen in earlier flow images in the *Z*-direction. A *Z*-directional velocity component, which is the out of plane, is shown in Fig. 8(*d*). The range for this velocity component is from -30 m/s to $+30$ m/s, and it signifies the importance of 3D flow measurements.

For most flow regimes, V_z is positive, indicating the air-flow from the intake valves to the exhaust valve. Most *Y*-directional and *Z*-directional velocities were generated by the valve lift, the suction

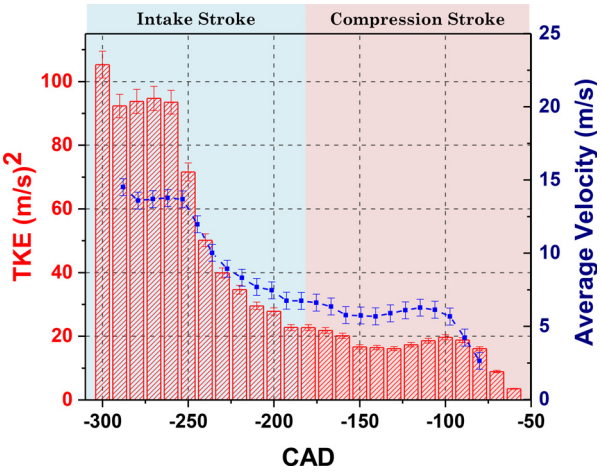

Fig. 10 Average TKE and average velocity profile from 300-deg CA to 60-deg CA

created by the downward moving piston, and flow reversals from the in-cylinder surfaces. Comparison of velocity components at mid-compression stroke indicates the existence of only *Z*-directional velocity components in most of the region. *X* and *Y* components of velocity were observed in the left regions of the flow and around the cylinder head. For rest of the regions, these velocity components were negligible (Fig. 9). The velocity components near the cylinder head are a result of flow compression and its reversal from the cylinder head. These lower values of *X* and *Y* components indicate that the absolute flow velocity of compression stroke is mostly due to out of plane flow velocity components.

Turbulent Kinetic Energy and Average Velocity Profile. Figure 10 shows the plot of average air velocity at $z = 0$ mm (below the injector plane) versus crank angle positions from 300-deg CA to 60-deg CA for an area of 36 mm × 25 mm. Average velocity calculations were done by averaging all velocity vectors in $z = 0$ mm plane. Due to physical constraints involving the experimental setup, average velocity and TKE analyses were limited up to 60-deg CA bTDC. However, variations of these parameters in entire intake stroke significantly affected the flow behavior in the compression stroke as well. Researchers reported that generating a significant vortical air-flow inside the combustion chamber during the intake stroke was one of the more promising ways to obtain high intensity turbulence in later part of the compression stroke and achieve a faster burning rate [30,31]. The average air velocity was in the range of 12–15 m/s upto the point of maximum valve lift, i.e., upto 255-deg CA. During the intake stroke, average air velocity decreased because of the energy dissipation due to flow interactions with the piston surface and cylinder walls. As the valves closed, average air velocity decreased almost linearly with crank angle upto the point of complete valve closure (i.e., at 133.5-deg CA). From this point onward (133.5-deg CA), the rate of air velocity decay reduced. This was possibly due to breakage of large-scale flow structures because of lower cylinder volume, which increased turbulence. The momentum imparted by the upward moving piston was another possible reason for lower average air velocity decay. From Fig. 10, it is also evident that the rate of energy dissipation was higher during the intake stroke compared to the compression stroke. The velocity fluctuations lowered in the compression stroke compared to the intake stroke. Semenov also reported similar results using HWA [7]. Average TKE was calculated using a mathematical expression given by Reuss [32]

$$\text{TKE} = \frac{1}{2}\rho V_{\text{rms}}^2 = \frac{1}{2}\rho u_{\text{rms}}^2 + \frac{1}{2}\rho v_{\text{rms}}^2 + \frac{1}{2}\rho w_{\text{rms}}^2$$

where, u, v, and w are the average velocity components in *X*, *Y*, and *Z*-directions, respectively (at $z = 0$ mm). Here, density ρ is assumed to be 1 kg/m^3 for air. Strength of flow has been indicated by average TKE. Higher TKE is a measure of strength of the airflow. Figure 10 shows that average TKE first increased during the intake stroke and then decreased with further downward movement of the piston. Huang et al. [33] also suggested that the strength of the swirl motion increased as the piston moved downward, and the swirl motion kept increasing during the first half of the compression stroke successively. This showed that flow behavior during late compression stroke was significantly affected by the flow strength during intake stroke and early compression stroke. During early intake stroke, intake valves opened and the piston accelerated downward. This increased the air velocity, which in-turn enhanced the TKE. After 270-deg CA, intake valve further opened, however, piston speed decreased, which resulted in relatively lower TKE. During the compression stroke, average TKE was much lower compared to the intake stroke because a major fraction of TKE dissipated due to internal friction of air flow/streams and cylinder–wall interactions. Dannemann et al. [18] also reported similar behavior of TKE in the compression stroke. They reported significantly smaller overall levels of TKE and a very smooth distribution of TKE in the compression stroke compared to the intake stroke.

Conclusions

Tomographic PIV was applied to a single-cylinder, four-valve optical research engine. The flow images of graphite-seeded intake air were taken in intake and compression stroke at 1200 rpm with a resolution of 2 CAD. Intake air flowfield showed flow velocities ranging from 0 to 60 m/s. Annular gap and higher piston speed in the first half of the intake stroke resulted in higher intake air velocities. Mostly, high speed flows were located between the two intake valves, which further collided with the piston top, resulting in the formation of recirculating flow structures. However, flow velocities decreased after the piston speed decreased from mid-intake position in the later part of intake stroke. During the compression stroke, velocity magnitude was significantly lower than the intake stroke. Most intake generated structures interacted with the in-cylinder surfaces, leading to viscous dissipation of flow energy. As the piston approached the TDC position in the compression stroke, upward moving piston squeezed air and provided upward momentum, which resulted in the formation of small recirculating flow patterns and slightly increased flow velocities. *Z*-directional variation of flowfield implied dependence of flow on its spatial location inside the engine cylinder. Strong incoming jet from the combined action of intake port created high velocity gradient in the exhaust valve region during the intake stroke, which resulted in the formation of cyclic structures. These structures ceased to exist in the compression stroke as the flow became more homogenous. At mid-intake stroke, all velocity components contributed to the absolute flow velocity. This particular port geometry (swirl port and tangential port) and strong incoming intake jet generated high flow velocities in *X* and *Y* directions, respectively. The existence of high velocities in *Z*-direction proved the need of 3D flow measurements. At mid-compression stroke, both *X* and *Y* velocity components almost ceased to exist except near the cylinder head. The mid-compression velocity was mostly contributed by the out of the plane velocity component, making it necessary to use 3D velocity measurement for better understanding the fuel–air mixing process. Average velocity profile suggested reduction in flow energy dissipation from the intake to the compression stroke. Study of average velocity profile suggested intake valve timing to be an important parameter in defining in-cylinder flows.

This study presented 3D, in-cylinder flow evolution in a single cylinder, four-valve, optical diesel engine at 1200 rpm at different crank angle positions during intake and compression stokes and

improved the understanding of in-cylinder flow evolution using Tomographic PIV.

Acknowledgment

Authors are thankful to Indian Institute of Technology Kanpur for providing financial support for setting-up this state-of-the-art single cylinder optical research engine facility for carrying out this study.

Nomenclature

V_x = velocity component in X-direction
V_y = velocity component in Y-direction
V_z = velocity component in Z-direction

References

[1] Maurya, R. K., and Agarwal, A. K., 2015, "Combustion and Emission Characterization of n-Butanol Fuelled HCCI Engine," ASME J. Energy Resour. Technol., **137**(1), p. 011101.
[2] Love, N. D., Parthasarathy, R. N., and Gollahalli, S. R., 2009, "Rapid Characterization of Radiation and Pollutant Emissions of Biodiesel and Hydrocarbon Liquid Fuels," ASME J. Energy Resour. Technol., **131**(1), p. 012202.
[3] Loüffler, G., Andahazy, D., Wartha, C., Winter, F., and Hofbauer, H., 2001, "NO_x and N_2O Formation Mechanisms—A Detailed Chemical Kinetic Modeling Study on a Single Fuel Particle in a Laboratory-Scale Fluidized Bed," ASME J. Energy Resour. Technol., **123**(3), pp. 228–235.
[4] Singh, A. P., and Agarwal, A. K., 2006, "Diesoline, Diesohol, and Diesosene Fuelled HCCI Engine Development," ASME J. Energy Resour. Technol., **138**(5), p. 052212.
[5] KidoguchI, Y., Yang, C., and Miwa, K., 1999, "Effect of High Squish Combustion Chamber on Simultaneous Reduction of NO_x and Particulate From a Direct-Injection Diesel Engine," SAE Paper No. 1999-01-1502.
[6] Bergstrand, P., and Denbratt, I., 2002, "The Effects of Leaner Charge and Swirl on Diesel Combustion," SAE Paper No. 2002-01-1633.
[7] Semenov, E. S., 1958, "Studies of Turbulent Gas Flow in Piston Engines," Otedelinie Technicheskikh Nauk, NASA Technical Translation F97, Report No. 8.
[8] Tutak, W., and Jamrozik, A., 1990, "Characteristics of the Flow Field in the Combustion Chamber of the Internal Combustion Test Engine," Chem. Process Eng., **32**(3), pp. 203–214.
[9] Catania, A. E., Dongiovanni, C., Mittica, A., Molina, G., and Spessa, E., 1995, "A New Test Bench for HWA Fluid-Dynamic Characterization of a Two-Valved In-Piston-Bowl Production Engine," SAE Paper No. 952467.
[10] Kang, K. Y., and Back, J. H., 1995, "LDV Measurement and Analysis of Tumble Formation and Decay in a Four-Valve Engine," Exp. Therm. Fluid Sci., **11**(2), pp. 181–189.
[11] Driver, T., Schinetsky, P., Davis, J., Drabo, M., Ölçmen, S. M., and Ashford, A., 2010, "Measurement and Analysis of Unsteady Flows in IC Engines," AIAA Paper No. 2010-1215.
[12] Novotný, J., and Manoch, L., 2010, "The Criterion of Choosing the Proper Seeding Particles," 18th International Conference on Engineering Mechanics, Svratka, Czech Republic, May 14–17, Paper No. 201, pp. 945–954.
[13] Hadad, T., and Gurka, R., 2013, "Effects of Particle Size, Concentration and Surface Coating on Turbulent Flow Properties Obtained Using PIV/PTV," Exp. Therm. Fluid Sci., **45**, pp. 203–212.
[14] Disch, C., Kubach, H., Spicher, U., Pfeil, J., Altenschmidt, F., and Schaupp, U., 2013, "Investigations of Spray-Induced Vortex Structures During Multiple Injections of a DISI Engine in Stratified Operation Using High-Speed-PIV," SAE Paper No. 2013-01-0563.
[15] Nishiyama, A., Jeong, H., Ikeda, Y., and Sawada, R., 2012, "Application of Endoscopic Stereo PIV to 3-D Exhaust Gas Flow Measurements in a Practical SI Engine," 16th International Symposium on Applications of Laser Techniques to Fluid Mechanics, Lisbon, Portugal, July 9–12, Paper No. 241.
[16] Sweetland, P., and Reitz, R. D., 1994, "Particle Image Velocimetry Measurements in the Piston Bowl of a DI Diesel Engine," SAE Paper No. 940283.
[17] Reeves, M., Towers, D. P., Tavender, B., and Buckberry, C. H., 1999, "A High-Speed All-Digital Technique for Cycle-Resolved 2-D Flow Measurement and Flow Visualization Within SI Engine Cylinders," Opt. Lasers Eng., **31**(4), pp. 247–261.
[18] Dannemann, J., Klaas, M., and Schröder, W., 2010, "Three Dimensional Flow Field Within a Four Valve Combustion Engine Measured by Particle-Image Velocimetry," 14th International Symposium on Flow Visualization (ISFV), EXCO Daegu, South Korea, June 21–24, pp. 21–24.
[19] Das, D. M., 2003, "Computational and Experimental Study of In-Cylinder Flow in a Direct Injection Gasoline (DIG) Engine," SAE Paper No. 2003-01-3083.
[20] Elsinga, G. E., Scarano, F., Wieneke, B., and Oudheusden, B. W. E., 2006, "Tomographic Particle Image Velocimetry," Exp. Fluids, **41**(6), pp. 933–947.
[21] Scarano, F., 2012, "Tomographic PIV: Principles and Practice," Meas. Sci., **24**(1), p. 012001.
[22] Baum, E., Peterson, B., Surmann, C., Michaelis, D., Böhm, B., and Dreizler, A., 2013, "Investigation of the 3-D Flow Field in an IC Engine Using Tomographic PIV," Proc. Combust. Inst., **34**(2), pp. 2903–2910.
[23] Overbrueggen, T., Klaas, M., Bahl, B., and Schroeder, W., 2015, "Tomographic Particle-Image Velocimetry Analysis of In-Cylinder Flows," SAE Int. J. Engines, **8**(3), pp. 1447–1467.
[24] Overbrüggen, T., Bücker, I., Dannemann, J., Karhoff, D. C., Klaas, M., and Schröder, W., 2015, "Planar Stereoscopic and Holographic PIV-Measurements of the In-Cylinder Flow of Combustion Engines," *Fuels from Biomass: An Interdisciplinary Approach*, Springer, Berlin, pp. 155–191.
[25] Singh, A. P., Gupta, A., and Agarwal, A. K., 2015, "Tomographic Particle Image Velocimetry for Flow Analysis in a Single Cylinder Optical Engine," SAE Int. J. Mater. Manuf., **8**(2), pp. 472–481.
[26] Singh, A. P., Gadekar, S., and Agarwal, A. K., 2016, "In-Cylinder Air-Flow Characteristics Using Tomographic PIV at Different Engine Speeds, Intake Air Temperatures and Intake Valve Deactivation in a Single Cylinder Optical Research Engine," SAE Paper No. 2016-28-0001.
[27] Foucher, F., Landry, L., Halter, F., and Mounaim-Rousselle, C., 2008, "Turbulent Flow Fields Analysis of a Spark-Ignition Engine as Function of the Boosted Pressure," 14th International Symposium on Applications of Laser Techniques to Fluid Mechanics, Lisbon, Portugal, July 7–10, Paper No. 12.2_3.
[28] Deslandes, W., Dupont, A., Georges, X. B., and Boree, C. J., 2003, "PIV Measurements of Internal Aerodynamic of Diesel Combustion Chamber," SAE Paper No. 2003-01-3083.
[29] Lumley, J. L., 1999, *Chapter 5: Flow in the Cylinder Engines—An introduction*, Cornell University, Cambridge University Press, Cambridge, UK.
[30] Heywood, J. B., 1987, "Fluid Motion Within the Cylinder of Internal Combustion Engines," ASME J. Fluids Eng., **109**(1), pp. 3–35.
[31] Heywood, J. B., 1988, *Internal Combustion Engine Fundamentals*, McGraw-Hill, New York.
[32] Reuss, D. L., 2000, "Cyclic Variability of Large-Scale Turbulent Structures in Directed and Undirected IC Engine Flows," SAE Paper No. 2000-01-0246.
[33] Huang, R. F., Huang, C. W., Chang, S. B., Yang, H. S., Lin, T. W., and Hsu, W. Y., 2005, "Topological Flow Evolutions in Cylinder of a Motored Engine During Intake and Compression Strokes," J. Fluids Struct., **20**(1), pp. 105–127.